J Comput Neurosci
DOI 10.1007/s10827-008-0086-6

# Retinal and cortical nonlinearities combine to produce masking in V1 responses to plaids

**Melinda Koelling · Robert Shapley · Michael Shelley**

Received: 23 January 2006 / Revised: 15 February 2008 / Accepted: 20 February 2008


**Abstract** The visual response of a cell in the primary visual cortex (V1) to a drifting grating stimulus at the cell's preferred orientation decreases when a second, perpendicular, grating is superimposed. This effect is called masking. To understand the nonlinear masking effect, we model the response of Macaque V1 simple cells in layer 4C$\alpha$ to input from magnocellular Lateral Geniculate Nucleus (LGN) cells. The cortical model network is a coarse-grained reduction of an integrate-and-fire network with excitation from LGN input and inhibition from other cortical neurons. The input is modeled as a sum of LGN cell responses. Each LGN cell is modeled as the convolution of a spatio-temporal filter with the visual stimulus, normalized by a retinal contrast gain control, and followed by rectification representing the LGN spike threshold. In our model, the experimentally observed masking arises at the level of LGN input to the cortex. The cortical network effectively induces a dynamic threshold that forces the test grating to have high contrast before it can overcome the masking provided by the perpendicular grating. The subcortical nonlinearities and the cortical network together account for the masking effect.

**Keywords** Functional organization and circuitry · Subcortical visual pathways · Visual masking

**Action Editor: Jonathan D. Victor**

Melinda Koelling is formerly from Center for Neural Science and Courant Institute, New York University.

M. Koelling (✉)
Department of Mathematics, Western Michigan University,
1903 Western Michigan Avenue,
Kalamazoo, MI 49008, USA
e-mail: melinda.koelling@wmich.edu

R. Shapley · M. Shelley
Center for Neural Science, New York University,
4 Washington Place, Room 809,
New York, NY 10003, USA

R. Shapley
e-mail: shapley@cns.nyu.edu

R. Shapley · M. Shelley
The Courant Institute, New York University,
251 Mercer Street, New York, NY 10012, USA

M. Shelley
e-mail: shelley@cims.nyu.edu

## 1 Introduction

Simple cells in mammalian visual cortex are sensitive to the orientation of patterns. Their response is roughly linear, at least for such elementary stimuli as drifting gratings or bars. The source of the near linearity is not obvious, and the form of the network that produces the near linearity has been the subject of ongoing debate. The model developed in McLaughlin et al. (2000) and Wielaard et al. (2001) has provided an anatomically motivated model network that reproduces the near linearity that helps explain the neural network in the visual cortex.

However, an investigation of the nonlinear aspects of simple cell response could help further illuminate the nature of the cortical network. It is true that in response to drifting grating stimuli at their preferred orientations, simple cells in primary visual cortex will typically increase their amplitude of firing with increases in stimulus contrast. When the drifting grating is not at the

preferred orientation, the increased response from the increased contrast is not as large as it was for preferred orientation, and when the grating is orthogonal to preferred, changes in the contrast have little or no effect on the responses of the cell. However, there is an effect of orthogonal-to-preferred stimuli. When preferred (*test*) and orthogonal (*mask*) gratings are superimposed to form a plaid, the cortical response to the plaid is less than that to the preferred grating alone. This nonlinear *masking* effect has been observed in cat primary visual cortex (V1) (Bonds 1989; Freeman et al. 2002) and macaque V1 (Carandini et al. 1997).

How might such masking arise? One possible source is the Lateral Geniculate Nucleus (LGN) input to V1 cortex. If so, then the mechanism is not obvious because unlike cortical cell responses, responses of cells in the LGN are not orientation selective. LGN cells respond equally strongly to visual grating stimuli at all angles and will respond more strongly to a plaid than to either of the two gratings alone (see for example Freeman et al. 2002). Hence, individual LGN cells do not exhibit masking behavior.

Although masking does not arise in individual LGN cells, masking could arise from the depression of thalamocortical synapses (see Carandini et al. 2002). Even though the response of LGN cells increases when the mask is added to the test, it is possible that the signal arriving at the cortical cell does not increase when mask is added to the test because synaptic potentials that arrive at a higher rate from the LGN become depressed in amplitude. Then the cortex would not have sufficient stimulation to make the cortex respond more to the masked stimulus than to the unmasked one.

However, thalamocortical depression is not the only possible nonlinear mechanism for masking. It is well known that the responses of individual retinal cells exhibit contrast gain control (see e.g. Shapley and Victor 1981). Therefore, it is possible that because of retinal contrast gain control the increase in response to test and mask shown simultaneously is not as great as the sum of the responses to test and mask individually. In this paper, we use a simplified model of a coarse-grained network (see Shelley and McLaughlin 2003) similar to the network model of McLaughlin et al. (2000) to investigate the possibility that, with retinal contrast gain control, the input from magnocellular LGN cells to the cortical network could explain the masking phenomenon as seen in macaque V1 (Carandini et al. 1997). The choice to construct a model of magnocellular LGN input to macaque V1 was motivated by the extensive experimental data on masking in macaque V1 (Carandini et al. 1997) which suggest that it is reasonable to expect that the qualitative response is determined mainly by magnocellular cells for the stimuli we consider. In the experiments, the contrast range extended from low values of 0.06 up to 0.5 contrast. The V1 cells chosen for analysis had responses over this range; specifically, what masking affected were contrast response functions that, in the control, unmasked condition, showed significantly large responses at low contrast. As originally argued in Carandini et al. (1997), this implies the masking data from the cells in the dataset were strongly influenced by their magnocellular input: the thalamocortical visual pathway that responds most to low contrast (Kaplan and Shapley 1982; Hicks et al. 1983). We show in our simplified model of V1 that retinal contrast gain control of the masking stimulus when combined with the recurrent cortical network can be sufficient to explain the experimentally observed cellular responses to masked stimuli in V1.

## 2 Methods

We model the response of Macaque 4C$\alpha$ simple cells to patterned visual stimuli. The input to V1 is modeled as a sum of individual LGN cell responses, and the response of an individual LGN cell is modeled as the convolution of a spatiotemporal filter with the intensity of the visual stimulus renormalized for retinal contrast gain control, followed by a rectification. The cortical network is represented by a coarse-grained reduction of a simple integrate-and-fire network in which excitation is provided by the geniculate input and inhibition is provided by the cortical network (McLaughlin et al. 2000; Shelley and McLaughlin 2003).

### 2.1 Stimulus

The fundamental stimulus is a *drifting grating*, the intensity of which at location $\mathbf{x}$ in the visual plane and at time $t$ is given by

$$I(\mathbf{x}, t) = I_0(1 + \epsilon \cos(2\pi(\omega t + \mathbf{k} \cdot \mathbf{x}) + \varphi)).$$

The vector $\mathbf{k}(\theta) = k\,(cos\theta, sin\theta)$ gives the grating's spatial frequency by its magnitude $k$ and the drift direction by its orientation $\theta$. The remaining parameters are temporal frequency $\omega$, spatial phase $\varphi$, and contrast $\epsilon \in [0, 1]$.

*Plaid stimuli* are the sum of two drifting gratings

$$I_0\big(1 + \epsilon_1 \cos(2\pi\,(\omega_1 t + \mathbf{k_1} \cdot \mathbf{x}) + \varphi_1) + \epsilon_2 \cos(2\pi\,(\omega_2 t + \mathbf{k_2} \cdot \mathbf{x}) + \varphi_2)\big),$$

where $\epsilon_1+\epsilon_2 \leq 1$ (as intensity can never be negative). In our studies, as in the experiments with which we compare our analytical results, the two drifting gratings in the plaid have the same temporal and spatial frequencies ($\omega_1 = \omega_2$ and $|\mathbf{k_1}| = |\mathbf{k_2}|$) and are perpendicular $\mathbf{k_1} \cdot \mathbf{k_2} = 0$).

## 2.2 LGN model

The firing rate $R$ of a single model LGN cell is determined by the convolution of the stimulus intensity $I(\mathbf{x}, t)$, normalized for retinal contrast gain control with a separable space-time kernel that is centered spatially at $\mathbf{y}$, the center of the cell's receptive field in the visual plane:

$$R(t, \mathbf{y}) = S\left(R_b \pm \int_{-\infty}^{t} ds \int_{\mathbf{x}\in R^2} d\mathbf{x}\, G(t-s) \times A(|\mathbf{x}-\mathbf{y}|)\frac{I(\mathbf{x}, s)}{I_0}\frac{\alpha}{\beta + \sqrt{\epsilon_1^2+\epsilon_2^2}}\right) \quad (1)$$

The temporal kernel $G$ and the spatial kernel $A$ are taken from Wielaard et al. (2001), who based their choice of kernels on the experimental data of Benardete and Kaplan (1999) and Reid and Shapley (2002).

The spatial kernel is given by

$$A(z) = \left\{\frac{a}{\pi\sigma_a^2}\exp\left(-\left|\frac{z}{\sigma_a}\right|^2\right) - \frac{b}{\pi\sigma_b^2}\exp\left(-\left|\frac{z}{\sigma_b}\right|^2\right)\right\},$$

where $(\sigma_a, \sigma_b) = (.066, .093)^o$ and where $(a, b) = (1, .74)$. The form of $A$ (a difference of Gaussians) is standard in the literature, the parameters are chosen to follow Wielaard et al. (2001), and the resulting $A$ is shown in Fig. 1. The temporal kernel $G$ is given by

$$G(t) = -t^5(\exp(-t/\tau_0) - c_1\exp(-t/\tau_1)),$$

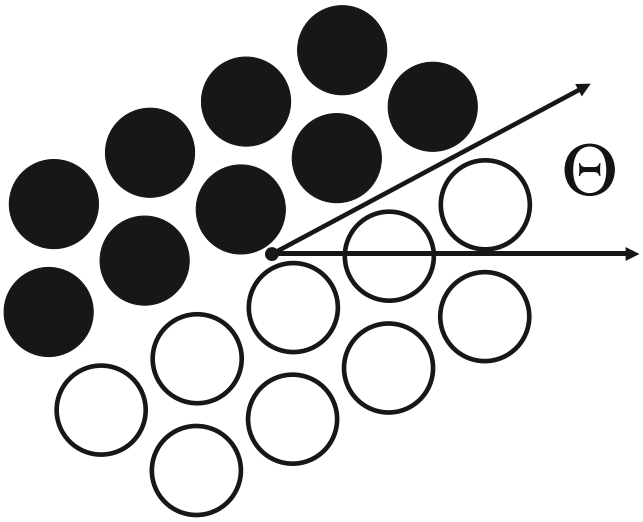


**Fig. 2** Basic layout of receptive field centers of LGN cells providing input to a single cortical cell. This layout is translated so that the origin is the center of the cortical cell's receptive field and rotated to obtain its angle preference. The *circles* indicate the center of the receptive field, *dark* indicate an off-centered cell and *light* indicates an on-centered cell

with $(\tau_0, \tau_1) = (3, 5)$ ms; $c_1$ is chosen so $G$ integrates to zero over $(0, \infty)$. Figure 1 also shows a graph of $G$. The variables $\alpha$, $\beta$ in Eq. (1) are chosen so that for a grating with frequencies 4 Hz and one cycle per degree, the response of LGN cells respond as observed in Shapley (1994). The rectification function is

$$S(r) = \begin{cases} 0 & r < 0 \\ r & r \geq 0. \end{cases}$$

Since there cannot be a negative response, $S$ must be zero for $r < 0$. The differing responses of On- and Off-center cells is captured by the choice of the sign preceding the integrals in Eq. (1).

For validation, Fig. 3 shows the response of a single model LGN cell to a drifting grating stimulus at

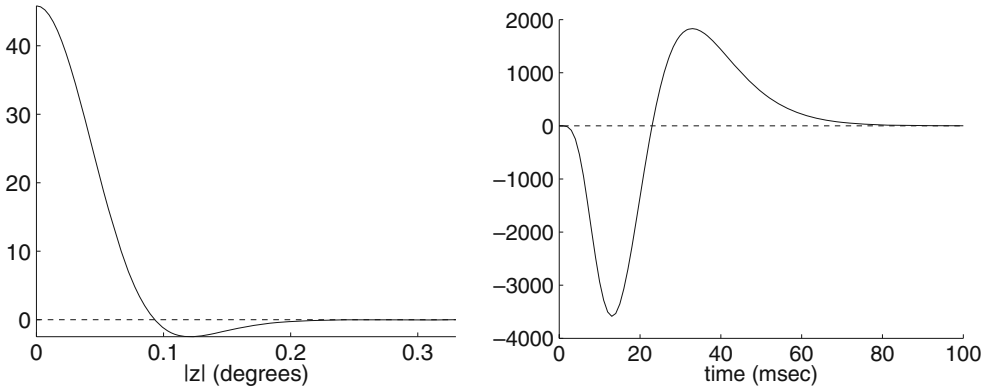


**Fig. 1** Responses of model LGN cells are the composition of a non-linear saturation and rectification function with a linear function involving a spatial and temporal convolution. Spatial kernel A (*left*), temporal kernel G (*right*). *Dashed line* indicates zero

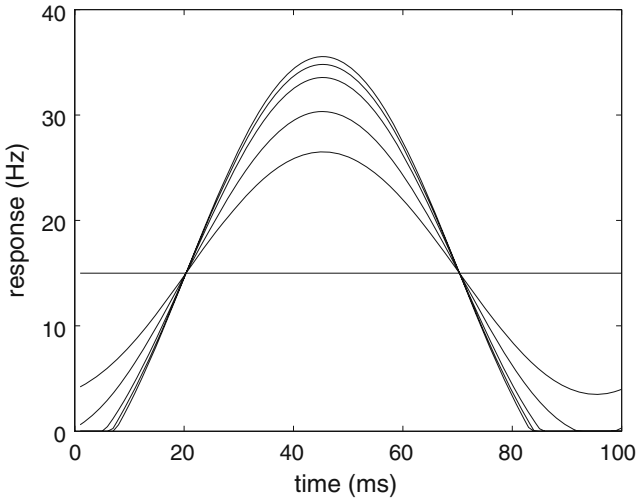


**Fig. 3** Temporal response of an LGN cell to drifting gratings of contrasts 0, 6, 12.5, 25, 37.7, 50%. Gratings at frequencies 4 Hz and 1 cycle per degree, as used in network simulations that follow (*right*)

contrasts of 0, 6, ...50% with 1 cycle/$^o$ spatial and 4 Hz temporal frequencies. In Fig. 4, we show the first Fourier component (amplitude) of the response as a function of contrast for both plots in Fig. 3. We also show data from real cells as approximated from Fig. 7 of Kaplan et al. (1987), Fig. 2 of Kaplan and Shapley (1986), and Fig. 4 of Shapley (1994). At 4 Hz, 1 cycle per degree, the model cells level off like those in Shapley (1994): both the highest value and rate at which the response levels off are similar.

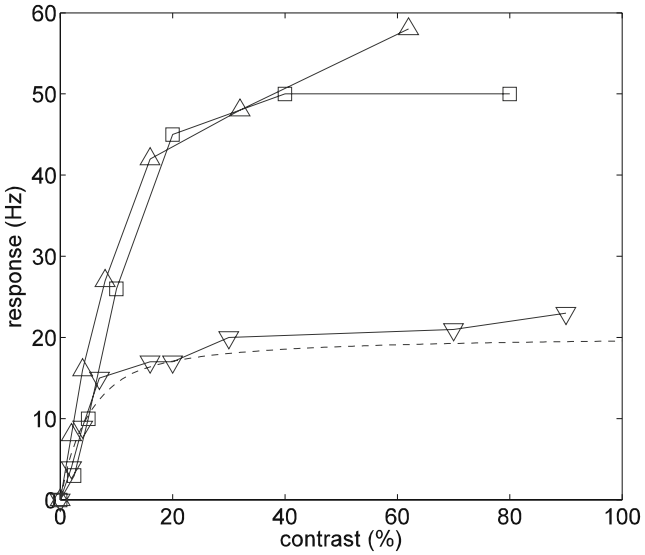


**Fig. 4** Amplitude of firing rate response of model and experimental LGN cells to drifting gratings of various contrasts. Model responses are drifting gratings of 4 Hz, 1 cycle/$^o$ (*dashed line*). Experimental data taken from Fig. 7 of Kaplan et al. (1987) (*upward triangle*) for a 4 Hz, 1 cycle/$^o$ signal, Kaplan and Shapley (1986) (*square*) for 4 Hz, optimal spatial frequency signal, Shapley (1994) (*downward triangle*) for a 4.22 Hz, 2.83 cycles/$^o$ signal

For the purpose of clarifying the graphs, we assume that all LGN cells have the same maximum response for most of this paper. It is more realistic to allow different LGN cells to have different maximum response values. In Fig. 4, the amplitude of our model cells level off at about 20 Hz, but the amplitudes of experimentally observed cells level off between 20 Hz and up to two or three times that value. To model this variability, we have also set different LGN cells to have different maximum response values uniformly distributed between one and two times the maximum response value for the model cells above. Because the graphs from this case depend on the random values, we first show results from LGN cells with non-random maximum responses, and then compare the results we obtain with the random maximum values.

The input to a single cortical cell from the LGN is the sum of the responses of a set of 18 LGN cells arranged as shown in Fig. 2, and has the form

$$g_{LGN}(t; \Theta, \Phi) = \sum_k R(t, y_k). \tag{2}$$

where the orientation and centering of this arrangement in the visual plane determines a preferred orientation $\Theta$ and spatial phase $\Phi$.

### 2.3 A simple cortical network model

The responses of a cortical network are modeled by a simplified coarse-grain reduction (Shelley and McLaughlin 2003) of an integrate-and-fire (I&F) network model of simple cells in V1 (see McLaughlin et al. 2000; Wielaard et al. 2001; Shelley and McLaughlin 2003). As was demonstrated in Wielaard et al., simple cell responses can arise through the interaction of geniculate excitation and a network inhibition that averages over the activity of surrounding cells that each receive geniculate excitation. When excitation and inhibition are balanced to yield reasonable firing rates, this network acted as a nonlinear amplitude filter on the geniculate excitation, yielding simple cell responses. We very briefly outline a coarse-grained version of the model in an all-to-all coupled setting.

To begin, the membrane potential $v$ of each model cortical cell is governed by

$$\begin{aligned} \frac{dv}{dt} &= -g_E \cdot (v - V_E) - g_I \cdot (v - V_I) - g_L v \\ &= -g_T (v - V_s) \end{aligned} \tag{3}$$

where $g_E, g_I$, are the excitatory and inhibitory membrane conductances, and $g_L$ is leakage conductances. All conductances have been divided by the membrane capacitance and hence have units of $sec^{-1}$. The potentials $V_E$ and $V_I$ are the associated reversal potentials, where the voltage has been normalized so that the leakage reversal potential is at zero, and spiking threshold is at unity. Under this rescaling, and using typical values of the reversal potentials Koch (1999), we have $V_E = 14/3$ and $V_I = -2/3$. Here $g_T = g_E + g_I + g_L$ is the *total conductance* and $V_S = (g_E V_E + g_I V_I)/g_T$ is the so-called *effective reversal potential*. The excitatory conductance has the form

$$g_E(t; \Theta, \Phi, f_E) = s_E \cdot g_{LGN}(t; \Theta, \Phi) + f_E, \tag{4}$$

where $g_{LGN}$ is given in Eq. (2), $s_E$ is the strength of the geniculate input, and $f_E$ is a noise term which models effects from outside the cortical and geniculate network described here. Differences in the responses of the model cortical cells to the same stimulus arise from differences in their geniculate contribution, such as preferred orientation $\Theta$ and the location of the receptive field center, represented by the spatial phase $\Phi$. Orientation preference affects how the cell responds to the orientation of the gratings in the plaid, and the location of the receptive field center affects how the cell responds to the phases of the gratings.

It is assumed that the inhibitory conductance input to a cortical cell, determined by the time-varying network activity in the form of spike mediated conductances changes, samples the outputs of many V1 neuronal subpopulations, with these subpopulations each having diverse preferred orientations $\Theta$, spatial phases $\Phi$, and external noise strengths. To reflect the consequent averaging of these functional parameters by the inhibitory membrane conductance, its form is taken as

$$\begin{aligned} g_I(t) &= s_I \int_{-\infty}^{t} ds\, G(t-s)\, \langle m \rangle_{\Theta,\Phi}(s) + f_I \\ &= s_I\, G * \langle m \rangle_{\Theta,\Phi}(t) + f_I, \end{aligned} \tag{5}$$

where $s_I$ represents the efficacy of network inhibition, and $G(t)$ models the conductance time-course of a GABA-mediated synapse, and has the form

$$G(t) = \begin{cases} (t/\tau^2)\exp(-t/\tau) & t \geq 0 \\ 0 & \text{otherwise} \end{cases} \tag{6}$$

with time-scale $\tau = 5$ ms. As above, $f_I$ represents an external noise contribution. The operation $\langle \cdot \rangle_{\Theta,\Phi}$ represents averaging the firing rates of these subpopulations over the distributions of these quantities, which is then filtered through the synaptic time-course. While our notation emphasizes the averaging over $\Theta$ and $\Phi$, averaging over external noise distributions is also included. The distributions of $\Theta$ and $\Phi$ are both taken as uniform over their domains of definition. Hence, in this model the network inhibition is global in orientation.

If the total conductance is high enough to yield a membrane time-scale smaller than the synaptic time scale, then an approximate solution can be obtained for $v$ in Eq. (3). Assuming this, we approximate the firing rate $m$ of a neuronal subpopulation by

$$m(t; \Theta, \Phi) = \mathcal{N}\left[g_{LGN}(t; \Theta, \Phi),\, G * \langle m \rangle_{\Theta,\Phi}(t)\right] \tag{7}$$

where

$$\mathcal{N} = \begin{cases} \frac{-g_T}{log\left(1 - V_S^{-1}\right)} & V_S > 1 \\ 0 & \text{otherwise} \end{cases} \tag{8}$$

Equation (7) closes as a dynamics for $\langle m \rangle_{\Theta,\Phi}$ by simply averaging, yielding

$$\langle m \rangle_{\Theta,\Phi}(t) = \left\langle \mathcal{N}\left[g_{LGN}(t; \Theta, \Phi),\, G * \langle m \rangle_{\Theta,\Phi}(t)\right] \right\rangle_{\Theta,\Phi} \tag{9}$$

Note that the averaging smoothes out the logarithmic onset of firing, as discussed in Shelley et al. (2002). Note too that with this choice of kernel $G$, the dynamics can be reposed as that of two coupled differential equations in time evolving $\langle m \rangle_{\Theta,\Phi}$. Finally, the averaging was over 8 phases per drifting grating (for a total of 64) and 8 angles of phase preference between zero and $\pi$. The noise distributions were taken to be Gaussians (specified below).

## 3 Results

We now investigate the responses of our model to plaid stimuli. The contrasts of the two perpendicular drifting gratings that compose the plaid are independently varied. Both gratings drift at a temporal frequency of 4 Hz and a spatial frequency of 1 cycle/$^o$. The excitatory noise term, $f_E$, is drawn from a Gaussian distribution with mean 6 and standard deviation 3, and the strength of the LGN input to the excitatory conductance, $s_E = 1/9$. The noise term $f_I$ is drawn from a Gaussian distribution with mean 85 and standard deviation 17.5, and the strength of network coupling in the inhibitory conductance, $s_I = 10$. We consider the response in three stages: the firing rate response of an individual LGN cell, the sum of the LGN firing rates which is the geniculate input to a cortical cell in the network, and the firing rate response of a cortical cell in the network.

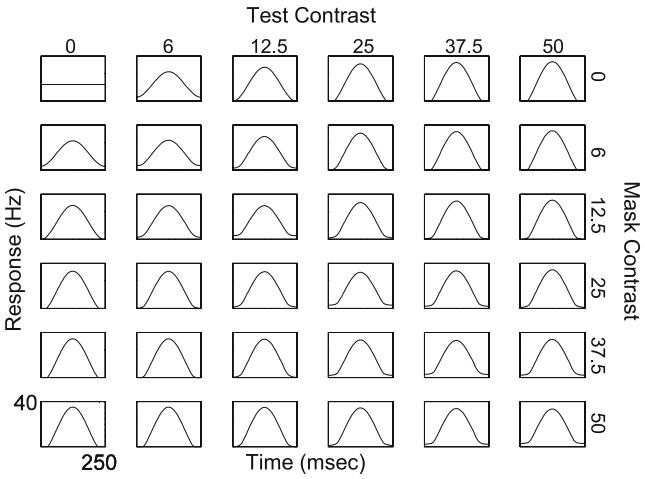


**Fig. 5** Firing rate responses of LGN cells to plaids of varying contrasts 0, 6, 12.5, 25, 37.5, and 50%, averaged over phase. *Rows* have constant contrast for one grating, leftmost is lowest contrast. *Columns* have constant contrast for the perpendicular grating, topmost is lowest contrast

**Individual LGN cells** First we consider the response of individual LGN cells to a plaid stimulus. The spatial phases of the gratings affect the firing rate response of the LGN cell in two different ways. First, spatial phases of the stimulus affect the temporal phases of the response, and second, they affect the shape of the response of the LGN cell, which depends on the portion of the plaid pattern that passes through the receptive field of the LGN neuron. In what follows, we only consider responses that have been averaged over phases of the plaid stimulus.

Figure 5 shows the response of an LGN cell for a variety of plaid contrasts. The rows correspond to contrast of one grating set to 0, 6, 12.5, 25, 37.5 and 50%, while the columns correspond to the perpendicular grating with contrast 0, 6, 12.5, 25, 37.5 and 50%. Each graph is the result of averaging over the phases of the gratings, where the average is taken by translating each response in time so the response attains its maximum at $t = 125$ ms. (The idea is to obtain the average response of the cell to a given pair of contrasts. We would like to separate the spatial phase from the change in shape; this determines our choice of average. Some translation is necessary to obtain a meaningful average: for example, if the responses are not translated at all before averaging, the average LGN response would be nearly constant in time.)

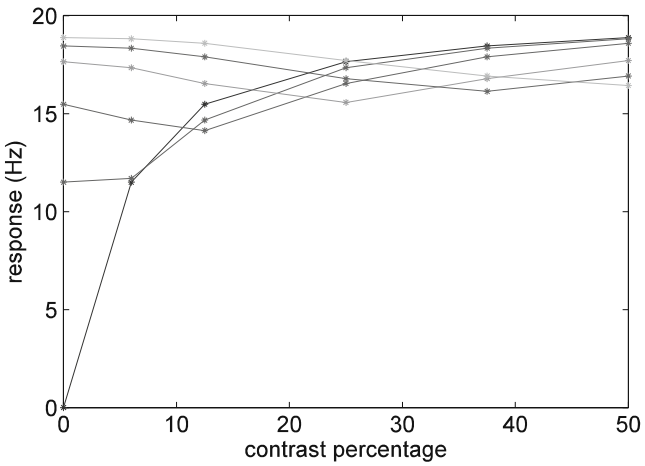


**Fig. 6** First Fourier component (amplitude) of the single LGN cell firing rate responses in Fig. 5 as a function of the contrast of one drifting grating. *Curves* correspond to holding the perpendicular drifting grating at fixed contrasts, 0, 6, 12.5, 25, 37.5, 50%

As a consequence of its lack of orientation selectivity, a single LGN cell responds equally to equal changes in the contrasts of two gratings: the single LGN cell gives the same response if grating one has contrast one and grating two has contrast two as it would if gratings one and two had contrasts two and one, respectively. The model LGN cell gives the experimentally observed response: for low contrasts, increasing the contrast of a grating increases response, and at higher contrasts, increasing the contrast has little effect, see e.g. Freeman et al. (2002).

The effect of changing the contrasts is further quantified in Fig. 6. One measure of response is the magnitude of its first temporal Fourier amplitude. This amplitude of the phase averaged response is a function of the two contrasts. Fixing one contrast, we plot the amplitude as a function of the contrast of the perpendicular grating. Comparing these curves, we can better understand the

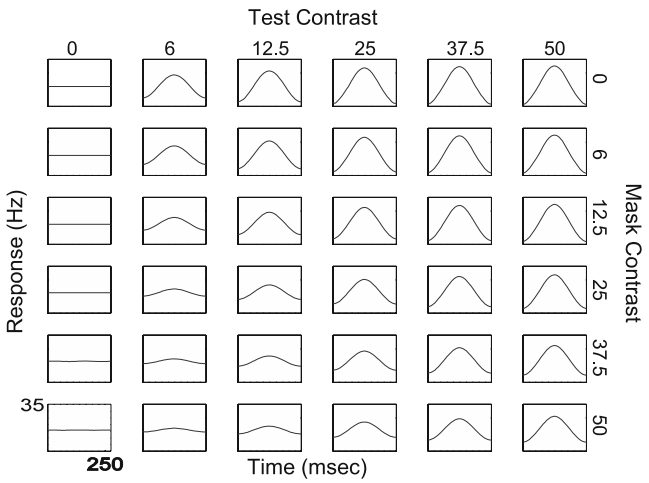


**Fig. 7** For various contrasts, firing rate response of the sum of LGN cells that input a cortical cell, averaged over phase. Contrasts are 0, 6, 12.5, 25, 37.5, and 50%. *Rows* have constant contrast for one grating, leftmost is lowest contrast. *Columns* have constant contrast for the perpendicular grating, topmost is lowest contrast. With increased contrast, the mean increases slightly

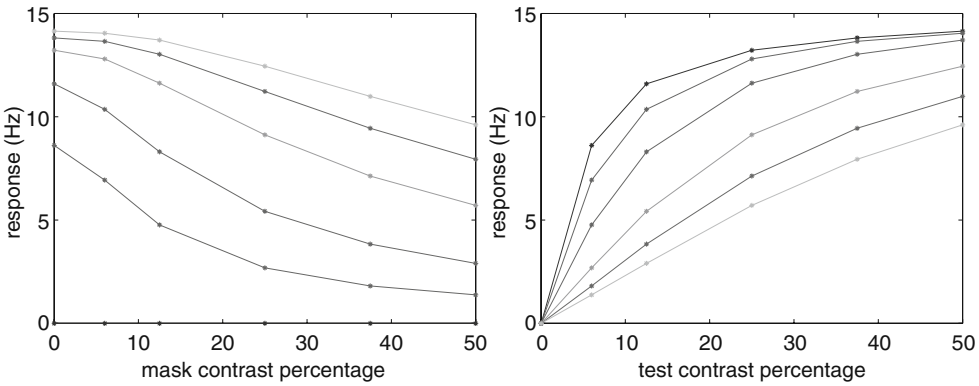


**Fig. 8** First Fourier component (amplitude) of the summed LGN firing rate response in Fig. 7 as a function of the contrast of one drifting grating. *Curves* correspond to holding the perpendicular drifting grating at a fixed contrast

effect of superimposing two gratings. When there is no perpendicular grating (i.e. the stimulus is a single drifting grating), the amplitude increases monotonically from zero and levels off. When the perpendicular grating has nonzero contrast (i.e. the stimulus is a plaid), the amplitude is always larger than that for zero contrast grating. As the contrast of the perpendicular grating increases, the amplitude of the response to the plaid increases until the amplitude is near the maximum value. If a plaid elicits a near maximum response, the effect of increasing the contrast of one of the gratings is negligible.

**Summed LGN input to V1** Next we investigate the geniculate input, the summed responses of 18 model LGN cells, to a model cortical cell. We note that the summation nearly removes dependence upon the phases of the plaid stimulus.

The phase-averaged response of the summed LGN input, for various stimulus contrasts, is given in Fig. 7. As in Fig. 5, rows and columns correspond to constant contrasts of two orthogonal gratings. They were chosen to be gratings in the preferred direction of the model cell (test) and the perpendicular (mask).

Unlike single LGN cells, the summed LGN input shows orientation selectivity in its modulation relative to its mean (the mean is unselective due to the radial symmetry in the receptive fields of individual LGN; see Sompolinsky and Shapley 1997; Troyer et al. 1998). This aspect is partially revealed by comparing test responses at 0% mask contrast, with mask responses at 0% test contrast. The response at orthogonal to preferred (mask response) is flat but has the same temporal mean as the modulating response at preferred (test response). Generally, increasing the test contrast at fixed mask contrast increases both the mean and the amplitude of the modulation of the response. Conversely, at fixed test contrast increasing the mask contrast decreases the firing rate modulation. For comparison, in Fig. 5, increasing either contrast of either grating from a low contrast value increases the oscillation, and values approach the maximum value for high contrast of both gratings.

The effect of contrast change on response modulation for the summed LGN input is further quantified in Fig. 8. The first Fourier component (amplitude) of the phase averaged response is plotted as a function of the stimulus contrasts. The amplitude of the phase-averaged response is given as a function of test contrast (right) and as a function of mask contrast (left). This is sharply different from the results shown in Fig. 6, where the response as a function of the contrast of either grating are identical. In this intermediate stage, the masking behavior reported in Carandini et al. (1997) and Freeman et al. (2002) begins to emerge. Increasing the test increases the response, and increasing the mask decreases the response. The amplitudes also level off at high test contrast in the figure on the right in Fig. 8.

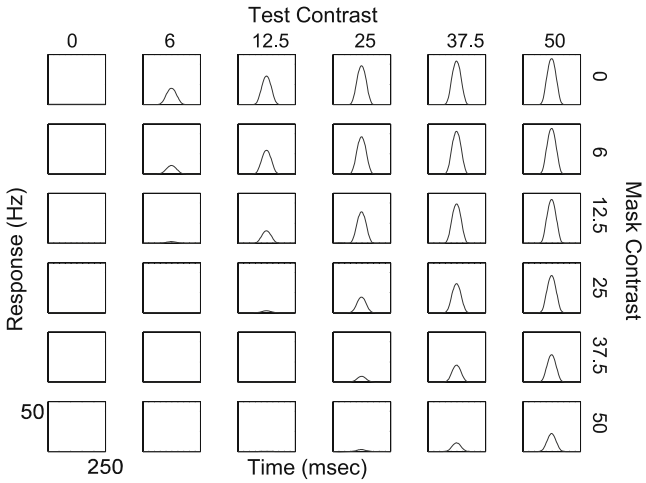


**Fig. 9** For various contrasts, firing rate response of a model V1 cell, averaged over phase. Contrasts are 0, 6, 12.5, 25, 37.5, and 50%. *Rows* have constant contrast for one grating, leftmost is lowest contrast. *Columns* have constant contrast for the perpendicular grating, topmost is lowest contrast

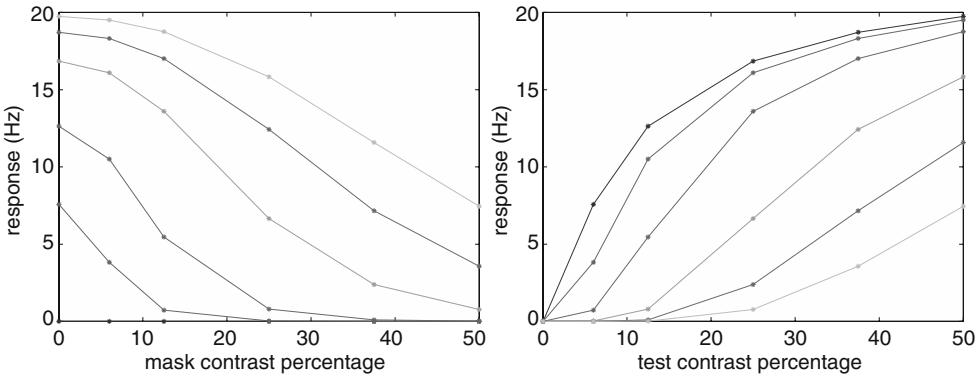


**Fig. 10** First Fourier component (amplitude) of the V1 firing rate response in Fig. 9 as a function of the contrast of one drifting grating. *Curves* correspond to holding the perpendicular drifting grating at a fixed contrast

**Cortical Response** Finally we consider the response of model cortical cells. The nonlinear rectification properties of the cortical network amplify the masking effect seen in the geniculate input to cortex. The cortical response to various stimulus contrasts is shown in Fig. 9. As with the geniculate input, the presence of the mask stimulus decreases the firing rate response from the response to the test stimulus alone. Higher mask contrast requires higher test contrast to produce non-zero firing rate. The masking effect is again further quantified by the F1 amplitudes, plotted in Fig. 10. In the left graph, the amplitude of the phase-averaged response is given as a function of mask contrast for various values of test contrast. In the right graph, the amplitude is given as a function of test contrast for various values of the mask contrast. Increasing the test increases the response, and increasing the mask decreases the response.

In addition, for high contrast and low mask, the changes in test contrast make little change in the firing rate response. The concavity of the amplitude of response for high mask contrasts and low test contrast seen in Freeman et al. (2002) is also exhibited by the model cells. For higher mask contrast and low test contrast, increases in test contrast have little effect on the firing rate. The firing rate response of V1 can in effect be obtained from dynamic thresholding of the summed LGN input and scaling the result. This will be discussed further in the discussion below.

To further understand the effect of the cortical network, compare the amplitudes from the input to a cortical cell in Fig. 8 to the amplitudes of response of a cortical cell in Fig. 10. The major difference between them is the change in concavity at low test contrast and high mask contrast. To demonstrate this, the input and response of a cortical cell from these figures is compared for 0% and 50% mask contrast and all test contrasts in Fig. 11. The inhibition in the network reduces firing for test signals of low contrast when the mask is of high contrast. When there is a drifting grating of high contrast in the plaid, the inhibitory conductance is high, but when there is no drifting grating of high contrast, the inhibitory conductance is low. This is independent of which grating produces the high inhibition because there are other neurons in the network for which the mask grating is preferred or near-preferred, and those neurons will be very active. In order for a neuron to fire, $V_s$ must be greater than one; see Eq. (8). So

$$0 < \frac{g_E + g_I + g_L}{g_E V_E + g_I V_I} < 1,$$

implying that

$$\frac{g_I(1 - V_I) + g_L}{V_E - 1} < g_E$$

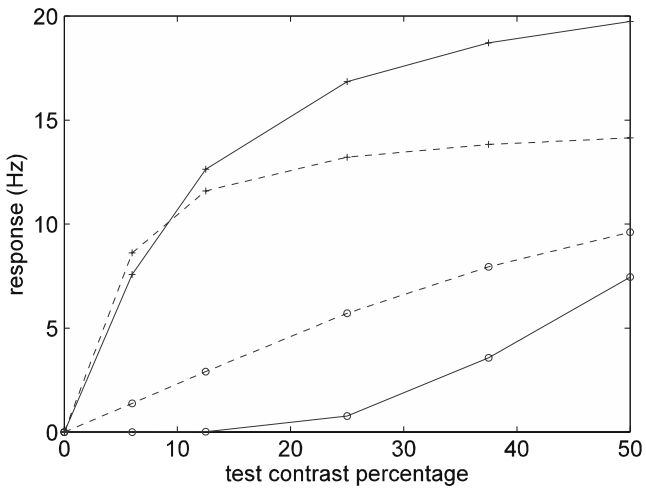


**Fig. 11** For various test contrasts, average amplitude of firing rate response of both the sum of LGN model cells that input a single V1 cell and a model V1 cell, averaged over phase. Response is shown for the both 0% and 50% mask. Test contrasts are 0, 6, 12.5, 25, 37.5, and 50%. The sum of the LGN model cells is marked by a *dashed line*; the response of a V1 cells is marked by a *solid line*. Mask contrast 0% is marked by a *plus sign*, mask contrast 50% is marked by a *circle*

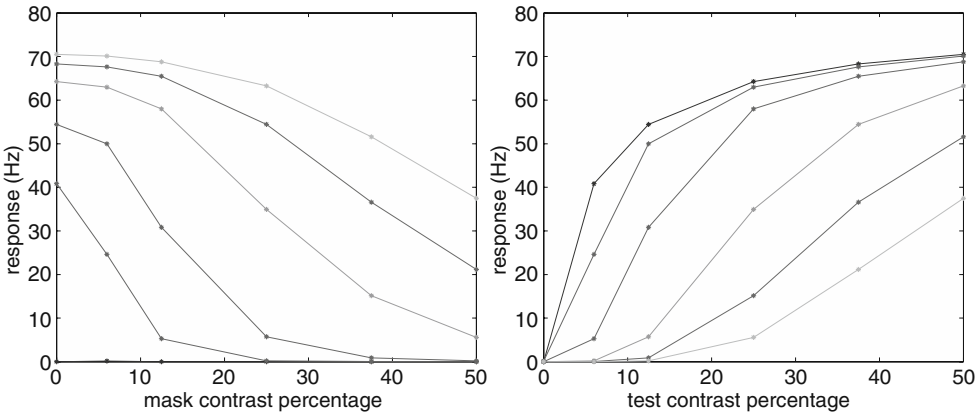


**Fig. 12** First Fourier component (amplitude) of the firing rate response as a function of one drifting grating, when the LGN cells giving input to the cortical cells have random maximum response values between one and two times the size of the maximum response values for the LGN cells in previous simulations. *Curves* correspond to holding the perpendicular drifting grating at a fixed contrast

for a neuron to fire. In other words, the inhibitory conductance determines a threshold for firing. In the case that there is a high contrast mask and a low contrast test, the inhibition is high enough to significantly reduce or eliminate the response to the test grating. The inhibition is shown in Fig. 13. The contrast of one grating is held constant while the contrast of the other increases. Only for both contrasts low is the inhibition low, which means only when mask contrast is low will the low test be able to produce a significant firing rate.

**Robustness** Our results appear robust. In the simulations above, we normalized our retinal contrast gain control so that an individual model LGN cell response leveled off as fast as the cells found in Shapley (1994), see Fig. 4, and we set all LGN cells to saturate at the same rate. We investigated the response of the model cortical cells at spatial and temporal frequencies which were not optimal. We have investigated several changes to this setup.

It is physically unreasonable to expect that all LGN cells responses level off to the same maximum value. This is evident in the experimental data we report in Fig. 4. All our model cells level off at an amplitude of about 20 Hz, but the amplitudes of experimental cells level off anywhere between 20 Hz (like ours) and 50 Hz. We have considered the case that the maximum response values for each LGN cell are randomly chosen between one and two times the maximum response value above. In this case, the cortical cells in this network still exhibit the masking effect, as shown in Fig. 12. Because the random values are higher than the non-random ones, the amplitudes of the V1 response can be higher, but the overall shape is preserved from Fig. 10 when the maximum response values were non-random.

It is also unreasonable to assume that all V1 cells have eighteen LGN cells providing them with thalamic input. We altered the footprint of the LGN cells that provide input to a cortical cell. Instead of taking the 18 cells as shown in Fig. 2, we looked at the response of cortical cells whose only thalamic input was two LGN cells. When we adjusted the strength of the LGN drive to be the same as before, the masking behavior was still evident.

In addition, we ran other tests. We have altered the frequencies of the signal by using frequencies which were optimal for the cortical cells. We have altered the retinal contrast gain control so that the LGN cells leveled off as fast as those shown in Kaplan and Shapley (1986), (see Fig. 4) and ran the code with spatial

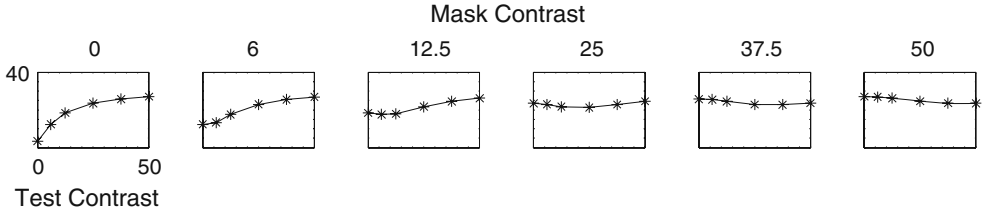


**Fig. 13** Average inhibitory conductances. In each *graph*, mask contrast is held constant at $0, 6, \ldots, 50\%$ (left to right). These are the contrasts labeled at the top of the figure. In each graph, the values of the inhibitory conductance are given when the test contrast is taken to be $0, 6, \ldots, 50\%$. In our computation, conductances are normalized to be dimensionless, so units are not given for the conductances. Unless both gratings are at low contrast, the inhibitory conductance is high

and temporal frequencies non-optimal. Under all these changes, the shapes of the summed LGN input to V1 and V1 response are robust, i.e. they are similar to the shapes in Figs. 8 and 10, respectively. The main difference between these different scenarios is that the firing rate has a different range of values. In summary, the retinal contrast gain control in the input to LGN causes the amplitudes of V1 responses to level off (Fig. 10), and the network's dynamic threshold provides the concavity change near zero.

## 4 Discussion

Our results show that retinal contrast gain control and an inhibitory cortical network can explain the masking nonlinearity that is observed experimentally in cortical response to plaids. We have used a coarse-grained reduction of an all-to-all coupled integrate-and-fire network. This network has excitation from the geniculate drive which is a sum of magnocellular LGN neurons and inhibition from the mean behavior of neurons in the network.

Experimentally, the amplitude of the response as a function of mask and test contrast is given in Freeman et al. (2002) (Fig. 2(a, b)) for cat visual cortex and Carandini et al. (1997) (Fig. 10(b, c)) for macaque V1. In our model, the masking observed in these experiments emerges at the level of the input from LGN to the cortex, see Fig. 8 above. The recurrent network amplifies the suppression of response by the mask at low test contrasts which produces concavity similar to that observed experimentally, see Fig. 10 above. What is proposed in this paper is a fairly simple and physiologically reasonable model of the geniculocortical response. We expect that a more detailed model would allow a more quantitative fit to the data. For example, we expect that the inclusion of parvocellular input from LGN in the model would not change the qualitative fit to the data but would improve the quantitative fit. Our work is based on macaque data, but the results depend on retinal contrast gain control and a simple cortical network that is dominated by inhibition. Since there is retinal contrast gain control in cat, such a model could equally well be used to describe the masking phenomenon in the responses of cat cortical neurons. The recent paper by Priebe and Ferster (2006) reaches a similar conclusion comparing a similar model and experimental data for the cat visual system.

In Freeman et al. (2002), the authors hypothesized that thalamocortical depression could also explain the masking behavior. Then in a later theoretical paper Carandini and colleagues presented a detailed analysis supporting the idea that the entire masking phenomenon was an expression of synaptic depression at the synapses from LGN to visual cortical cells (Carandini et al. 2002). The argument for synaptic depression as the sole mechanism for masking was based on the assumption that the LGN response to plaid stimuli was completely linear, and all the nonlinearity of masking was because of depression. This argument was not supported by experimental data from the same group (Freeman et al. 2002) about the cat LGN, nor by experimental data from the macaque LGN (e.g. Kaplan et al. 1987). The theoretical analysis in this paper indicates that there is no need for synaptic depression to play any role in the nonlinear masking phenomenon, and that the nonlinearity of LGN responses seen in the experimental data coupled into a recurrent cortical network accounts satisfactorily for the masking phenomenon. This theoretical result is strongly supported by the results of Boudreau and Ferster that indicate that there is very little modulation by visual stimulation of synaptic depression in the thalamocortical LGN $\rightarrow$ V1 synapses (Boudreau and Ferster 2005).

There have been several prior explanations of cross-orientation masking based on cortico-cortical inhibition that is broadly tuned for orientation (e.g., Bonds 1989; Carandini et al. 1997). Lauritzen et al. (2001) offer a theory for cross-orientation masking based on a model with cortical feedforward inhibition much more broadly tuned in orientation than cortico-cortical excitation. The results of Freeman et al. (2002) however indicate that cross-orientation masking is not only a result of cortical interactions. Nevertheless, we found that the fit of our model in a particular part of the contrast-response curves, in the low-response region, was improved by including cortico-cortical inhibition, as pointed out in Results. The idea that there is local cortico-cortical inhibition across orientation is a venerable idea that has been proposed many times to explain many observations (Grossberg 1975; Heeger 1992). Such broadly tuned inhibition also emerges in a realistic, large-scale model of the V1 network and can be used to explain the properties of orientation selectivity (McLaughlin et al. 2000).

While cross-orientation masking now appears not to depend only on cortical cross-orientation inhibition, there are many experimental data that suggest inhibition's functional importance in the visual cortex. Reverse correlation experiments that measure the dynamics of orientation selectivity in macaque V1 neurons reveal a slightly delayed suppressive effect that is very broadly tuned for orientation (Ringach et al. 1997; Xing et al. 2005). This untuned suppression was interpreted as cortical inhibition (Xing et al. 2005). It

contributes significantly to increasing orientation selectivity in the dynamics experiments. Another result from a separate line of inquiry is the demonstration of inhibitory conductance more broadly tuned (in orientation) than excitatory conductance, observed in intracellular recordings from cat striate cortex neurons (Anderson et al. 2000; Monier et al. 2003). Additional evidence for the role of cortical inhibition comes from Sato et al. (1996) who found that neuronal orientation selectivity was reduced in macaque V1 when GABAergic inhibition was blocked (cf. especially Fig. 8 in Sato et al. 1996) Therefore, one should not conclude that there is no cross-orientation inhibition just because we have shown that inhibition is not needed to explain most of the observed cross-orientation masking.

**Acknowledgements** M.K. gratefully acknowledges support from NEI Computational Training Grant T32 EY 7158, and R.S. acknowledges support from the Sloan and Swartz Foundations for the NYU Theoretical Neuroscience Program.

## References

Anderson, J. S., Carandini, M., & Ferster, D. (2000). Orientation tuning of input conductance, excitation, and inhibition in cat primary visual cortex. *Journal of Neurophysiology*, *84*, 909–926.

Benardete, E., & Kaplan, E. (1999). The dynamics of primate [m] retinal ganglion cells. *Visual Neuroscience*, *16*, 355–368.

Bonds, A. B. (1989). Role of inhibition in the specification of orientation selectivity of cells in the cat striate cortex. *Visual Neuroscience*, *2*, 41–55.

Boudreau, C. E., & Ferster, D. (2005). Short-term depression in thalamocortical synapses of cat primary visual cortex. *Journal of Neuroscience*, *25*, 7179–7190.

Carandini, M., Heeger, D. J., & Movshon, J. A. (1997). Linearity and normalization in simple cells of the macaque primary visual cortex. *Journal of Neuroscience*, *17*(21), 8621–8644.

Carandini, M., Heeger, D. J., Senn, W. (2002). A synaptic explanation of suppression in visual cortex. *Journal of Neuroscience*, *22*, 10053–10065

Freeman, T. C. B., Durand, S., Kiper, D. C., & Carandini, M. (2002). Suppression without inhibition in visual cortex. *Neuron*, *35*, 759–771.

Grossberg, S. (1975). On the development of feature detectors in the visual cortex with applications to learning and reaction-diffusion systems. *Biological Cybernetics, 21*, 145–159.

Heeger, D. (1992). Normalization of cell responses in cat striate cortex. *Visual Neuroscience*, *9*, 181–97.

Hicks, T. P., Lee, B. B., & Vidyasagar, T. R. (1983). The responses of cells in macaque lateral geniculate nucleus to sinusoidal gratings. *Journal of Physiology*, *337*, 183–200.

Kaplan, E., Purpura, K., & Shapley, R. (1987). Contrast affects the transmission of visual information through the mammalian lateral geniculate nucleas. *Journal of Physiology*, *391*, 267–288.

Kaplan, E., & Shapley, R. (1982). X and Y cells in he laterial geniculate nucleus of macaque monkeys. *Journal of Physiology*, *330*, 125–143.

Kaplan, E., & Shapley, R. (1986). The primate retina contains two types of ganglion cells, with hight and low contrast sensitivity. *Proceedings of the National Academy of Sciences*, *83*, 2755–2757.

Koch, C. (1999). *Biophysics of computation*. Oxford: Oxford University Press.

Lauritzen, T. Z., Krukowski, A. E., & Miller, K. D. (2001). Local correlation-based circuitry can account for responses to multi-grating stimuli in a model of cat v1. *Journal of Neurophysiology*, *86*, 1803–1815.

McLaughlin, D., Shapley, R., Shelley, M., & Wielaard, D. J. (2000). A neuronal network model of macaque primary visual cortex (v1): Orientation tuning and dynamics in the input layer 4calpha. *Proceedings of the National Academy of Sciences*, *97*, 8087–8092.

Monier, C., Chavane, F., Baudot, P., Graham, L. J., & Fregnac, Y. (2003). Orientation and direction selectivity of synaptic inputs in visual cortical neurons: A diversity of combinations produces spike tuning. *Neuron*, *37*, 663–680.

Priebe, N. J., Ferster, D. (2006). Mechanisms underlying cross-orientation suppression in cat visual cortex. *Nature Neuroscience*, *9*, 552–561 (2006)

Reid, R. C., & Shapley, R. M. (2002). Space and time maps of cone photoreceptor signals in macaque lateral geniculate nucleus. *Journal of Neuroscience*, *22*, 6158–6175.

Ringach, D. L., Hawken, M. J., & Shapley, R. (1997). Dynamics of orientation tuning in macaque primary visual cortex. *Nature*, *387*, 281–284.

Sato, H., Katsuyama, N., Tamura, H., Hata, Y., & Tsumoto, T. (1996). Mechanisms underlying orientation selectivity of neurons in the primary visual cortex of the macaque. *Journal of Physiology*, *494*, 757–771.

Shapley, R. (1994). Linearity and non-linearity in cortical receptive fields. In: Higher order processing in the visual system, Ciba Symposium 184. Chichester: Wiley.

Shapley, R. M., & Victor, J. D. (1981). How the contrast gain control modifies the frequency responses of cat retinal ganglion cells. *Journal of Physiology*, *318*, 161–179.

Shelley, M., & McLaughlin, D. (2003). Coarse grained reduction and analysis of a network model of cortical response I: Drifting grating stimuli. *Journal of Comparative Neuroscience*, *13*, 97–122.

Shelley, M., McLaughlin, D., Shapley, R., & Wielaard, J. (2002). States of high conductance in a large-scale model of the visual cortex. *Journal of Comparative Neuroscience, 13*, 93–109.

Sompolinsky, H., & Shapley, R. (1997). New perspectives on the mechanisms for orientation selectivity. *Current Opinion in Neurobiology, 7*, 514–522.

Troyer, T., Krukowski, A., Priebe, N., & Miller, K. (1998). Contrast invariant orientation tuning in cat visual cortex with feedforward tuning and correlation based intracortical connectivity. *Journal of Neuroscience*, *18*, 5908–5927.

Xing, D., Shapley, R. M., Hawken, M. J., & Ringach, D. L. (2005). Effect of stimulus size on the dynamics of orientation selectivity in macaque v1. *Journal of Neurophysiology*, *94*, 799–812.

Wielaard, D. J., Shelley, M., McLaughlin, D., & Shapley, R. (2001). How simple cells are made in a nonlinear network model of the visual cortex. *Journal of Neuroscience*, *21*(14), 5203–5311.